processes

MDPI

Article

Optimal Layout Methods for Deep Chamber to Separate Coal and Gangue Based on the Weak Stratum Horizon

Cheng Zhu [1,*], Yong Yuan [2,3,*], Hanqing Sun [1], Zhongshun Chen [2,3] and Wenmiao Wang [2,3]

[1] School of Civil Engineering and Transportation, South China University of Technology, Guangzhou 510641, China; sunhanqing@whu.edu.cn
[2] Key Laboratory of Deep Coal Resource Mining, Ministry of Education of China, China University of Mining and Technology, Xuzhou 221116, China; chenzhongshun2016@163.com (Z.C.); wwmdx1108@163.com (W.W.)
[3] School of Mines, China University of Mining and Technology, Xuzhou 221116, China
* Correspondence: zhuchengcumt@163.com (C.Z.); yy20062006@163.com (Y.Y.)

Abstract: Aiming at the optimal layout of a deep chamber for coal–gangue separation (DCCS) based on the weak stratum horizon, an in-depth study was carried out by combining field investigations, model tests, and numerical simulations. Firstly, the main structural characteristics of DCCS were summarized. Then, the deformation and failure law for rocks surrounding DCCS were revealed under different horizons in the weak stratum. Finally, the optimal layout methods of DCCS based on the thickness and horizon in the weak stratum were determined in different in situ stresses, using the proposed comprehensive evaluation method for surrounding-rock stability. The results show that if the thickness of the weak stratum was small, the side near the roof of DCCS should be arranged along the weak stratum when the lateral pressure coefficient was $\lambda < 0.6$ or $\lambda > 1$. The side near the floor of DCCS was arranged along the weak stratum when $0.6 \leq \lambda \leq 1$ and the surrounding-rock stability was the best. If the thickness of the weak stratum was large, the side of DCCS should be arranged along the weak stratum when $\lambda < 0.6$ or $\lambda > 1$. The floor of DCCS was arranged along the weak stratum when $0.6 \leq \lambda \leq 1$, which was most favorable for the surrounding-rock control. The research results have important guiding significance for the spatial layout and support design of DCCS.

Keywords: coal–gangue separation chamber; structure characteristics; weak stratum horizon; deformation and failure law; optimal layout methods

Citation: Zhu, C.; Yuan, Y.; Sun, H.; Chen, Z.; Wang, W. Optimal Layout Methods for Deep Chamber to Separate Coal and Gangue Based on the Weak Stratum Horizon. *Processes* **2023**, *11*, 2484. https://doi.org/10.3390/pr11082484

Academic Editor: Raymond Cecil Everson

Received: 4 July 2023
Revised: 3 August 2023
Accepted: 16 August 2023
Published: 18 August 2023

1. Introduction

Deep mining has become the norm in coal resource development in China since the increasing depletion of shallow resources [1,2]. At present, coal preparation is directly completed underground in many deep mines to solve problems, such as increased gangue production, reduced efficiency of mine hoisting, gangue discharge, and surface subsidence [3,4]. The separated gangue is directly backfilled in the goaf, whereby, underground mining, dressing, and backfilling have been integrated (Figure 1) [5–8]. The deep chamber for coal–gangue separation (DCCS) is an important place for underground coal preparation. Therefore, the long-term stability in controlling the rocks surrounding DCCS can ensure the efficient operation of the integrated system of mining, dressing, and backfilling [9].

The ideal spatial location of DCCS is in a stable rock stratum with high strength and large thickness close to the mined seam. It can reduce the damage range and difficulties in supporting the surrounding rocks. In fact, the height of DCCS is relatively large (generally greater than 7.0 m), and there is often no thick or hard rock stratum in the coal measure strata [10]. Therefore, the surface surrounding rocks of DCCS is generally composed of multiple rock strata. The surrounding-rock stability of DCCS is directly controlled by the composition conditions of the surrounding rocks, especially the horizon of the weak stratum (e.g., mudstone, argillaceous sandstone, and sandy mudstone). At present, research on the spatial layout of chambers in coal mining mainly considers factors such as in situ

stress environment, excavation of adjacent chambers, and mining influence of the adjacent working face [8,11–13]. Meanwhile, studies on the influence of a weak stratum on the surrounding rock stability of the chamber mainly focus on the failure mechanism and reinforcement countermeasures of the weak stratum [14,15]. However, there are still few reports on the optimal layout methods of chambers based on the horizon of the weak stratum. Therefore, an in-depth exploration is required for the above issues.

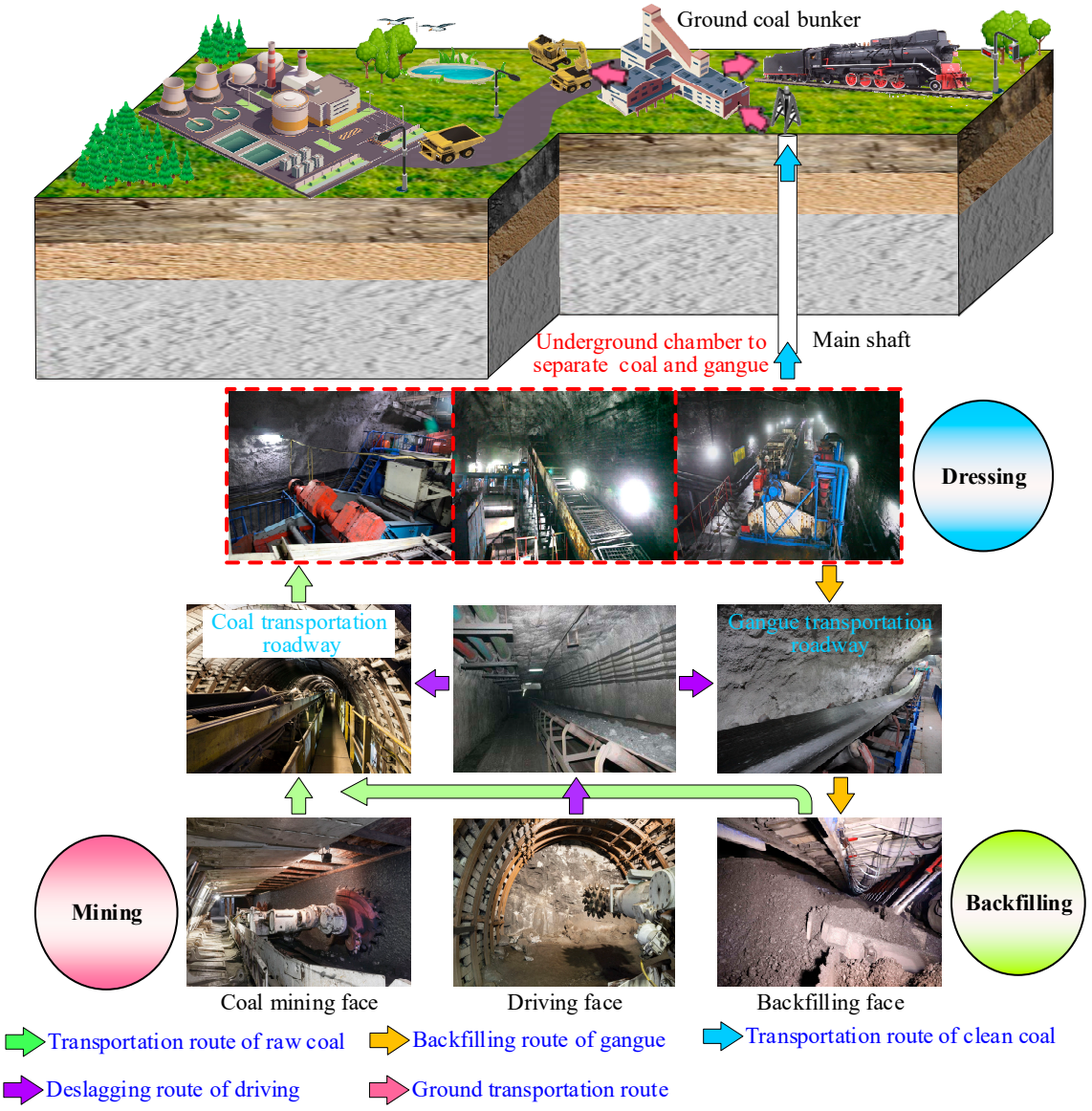

Figure 1. Integrated technology for mining, dressing, and backfilling.

The main structural characteristics of DCCS were summarized according to the field investigation data in the work. Then, the deformation and failure law of rocks surrounding the DCCS under different horizons in the weak stratum were revealed by a similar simulation test. Finally, 60 sets of numerical simulation schemes were designed by considering the lateral pressure coefficient as well as the thickness and horizon of the weak stratum. The optimal layout methods of DCCS based on the horizon of the weak stratum in different in situ stress environments were determined according to the proposed comprehensive evaluation method of surrounding-rock stability. The research results can provide important references for the spatial layout and support design of DCCS and have broad application prospects in deep resource mining.

2. General Engineering Background

Chambers in Chinese coal mines are defined as underground roadways with specific functional uses, including substations, pump rooms, and winch rooms. The development of underground mechanical equipment has led to new requirements for the spatial structures of chambers, which must now be designed to accommodate large-scale, intensive, and intelligent machinery [16]. Figure 2 shows the underground chamber for coal–gangue separation at Longgu Coal Mine, Pingdingshan 12# Coal Mine, and Binhu Coal Mine [6,8]. Table 1 shows the spatial size statistics for chambers of coal–gangue separations. DCCS is characterized by its large section size, elongated cross-sectional shape, and significant difference between the axial length and section size due to the centralized placement of coal dressing, disintermediation, media recycling, and other equipment.

Figure 2. Underground chamber for coal–gangue separation.

Table 1. Size statistics of underground chambers for coal–gangue separation.

Name of Coal Mine	Coal Preparation Technology	Name of Chamber	Section Shape	Width × Height (m)	Width-to-Height Ratio	Axial Length (m)
Longgu Coal Mine	Heavy medium shallow trough	Chamber of gangue discharge	Three centered arch	7.5 × 9.0	0.83	85.6
Pingdingshan 12# Coal Mine		Washing chamber	Semi-circular arch	8.0 × 9.2	0.87	75.0
Jiyang Coal Mine		Chamber of gangue discharge		6.8 × 7.0	0.97	70.0
Binhu Coal Mine	X-ray	Chamber of coal-gangue separation		5.5 × 7.4	0.74	41.0
Tangshan Coal Mine	Moving screen jigging	Chamber of jigging separation		6.2 × 9.3	0.67	25.8
Xiezhuang Coal Mine				6.5 × 7.5	0.87	25.0

At present, there is no standardized classification standard for the chamber section in coal mining. Some researchers have proposed that the chamber section can be divided into a small section (<8 m^2), medium section (8–12 m^2), large section (12–20 m^2), and super large section (≥20 m^2), according to the sectional area [17]. Some researchers have also recommended dividing the chamber section into a super small section (<3 m^2), small section (3–10 m^2), medium section (10–50 m^2), large section (50–100 m^2), and super large section (≥100 m^2), according to the section classification recommendations proposed by the International Tunneling Association [18]. Other researchers divided the chamber section into a small section (≤3 m), medium section (3.1–4 m), large section (4.1–5 m), and super large section (≥5.1 m), according to the span [19]. Meanwhile, it is generally believed that the reasonable ratio of width to height in the chamber is 1–1.2. For example, the width of the main roadway in the Lu'an mining area is generally 4.0–5.5 m, and the height is 3.5–4.5 m [20,21]. The general width of the roadway is 5.0–6.5 m and the height is 3.5–4.5 m in the Shandong mining area [22,23]. Accordingly, when the ratio of width to height is less than 1, it is referred to as the small width-to-height ratio in the work.

In summary, DCCS exhibits the structural characteristics of a large section (super large section), small width-to-height ratio, and axial length significantly greater than

the section size. These features distinguish it from both the underground roadway and traditional chamber.

When the surface surrounding rocks of DCCS contain a single weak stratum, there are various situations on its horizon (Figure 3). A research method that combines similar simulation tests and numerical simulations is used to study the influence of the weak-stratum horizon on the surrounding-rock stability of DCCS. Models 1 and 2 are mainly used as comparative references. Models 3 to 8 are used to analyze the weak stratum with large thicknesses, while models 9 to 15 are used to study the weak stratum with small thicknesses.

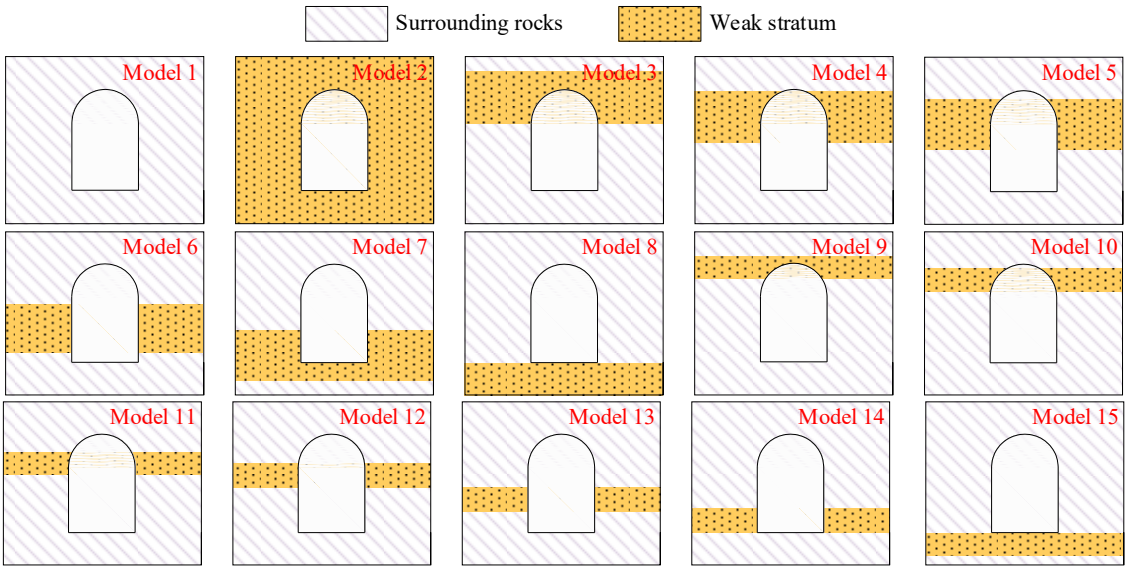

Figure 3. Models of different horizons of a single weak stratum.

3. Similar Simulation Tests

A similar simulation test involves creating a physical model of the actual mine prototype at a certain scale, and then, conducting excavations within the model. The mechanical phenomena occurring in the mine prototype and the distribution law of rock pressure can be inferred by observing the deformation, displacement, failure, and pressure of rock strata. Therefore, similar simulation tests can be used to analyze the deformation and failure law in rocks surrounding DCCS under different horizons of the weak stratum. Meanwhile, the focus of the work was to determine the optimal layout methods of DCCS based on the weak-stratum horizon in different in situ stress environments. The lateral pressure coefficient should be considered an important factor. If only similar simulation tests are conducted, it is imperative to have model frames with adjustable lateral pressure and a large number of models to be laid, which results in a substantial workload. Numerical simulations can solve the above problems. Additionally, the test results can be mutually verified by the numerical simulation results.

The axial length of DCCS is significantly larger than its section size, meaning the plane-strain similarity model is selected. If all the models in Figure 3 are used for similar simulation tests, the workload becomes huge. The tests can only be carried out in batches due to the limited number of plane-strain model frames in the laboratory, which makes it difficult to ensure consistency. Therefore, only representative models are selected for simulation tests. The weak stratum is located in the roof, side, and floor of DCCS in sequence in models 3, 6, and 8. Simulation tests are performed for the above three model sets to analyze the typical failure situations in the weak stratum in different areas of DCCS. Meanwhile, the deformation and failure patterns in the weak stratum and its adjacent surrounding rocks can be more intuitively presented during the simulation tests because of

the large thickness of the weak stratum in the three model sets. Therefore, models 3, 6, and 8 are finally selected for the simulation tests.

3.1. Determination of Similar Parameters

According to the similarity theory, test models should ideally be similar to all physical quantities in engineering practices [24]. However, it is difficult to achieve in testing. The geological mechanics model and prototype only need to satisfy geometric and stress similarities [25,26]. The similarity model and prototype should meet the following requirements based on the π law of the similarity theory.

$$(P/E)_p = (P/E)_m \tag{1}$$

$$(\sigma/E)_p = (\sigma/E)_m \tag{2}$$

$$(\delta/L)_p = (\delta/L)_m \tag{3}$$

$$(R/E)_p = (R/E)_m \tag{4}$$

$$(\sigma/L\gamma)_p = (\sigma/L\gamma)_m \tag{5}$$

where P is the load on the rock mass, MPa; E is the elastic modulus of the rock mass, MPa; σ is the stress in the rock mass, MPa; δ is the deformation of the rock mass, m; L is the geometric dimension, m; R is the strength of the rock mass, MPa; γ is the bulk density of the rock mass, kN/m^3.

Based on Equations (1)–(5) [27],

$$C_\delta = C_L \tag{6}$$

$$C_p = C_\sigma = C_E = C_R = C_L C_\gamma \tag{7}$$

where C_L is the similarity ratio of geometric dimensions; C_γ is the similarity ratio of the bulk density; C_δ is the similarity ratio of the deformation; C_p is the similarity ratio of the load; C_σ is the similarity ratio of the stress; C_E is the similarity ratio of the elastic modulus; C_R is the similarity ratio of strength.

C_L should be determined according to the actual sizes of DCCS and plane-strain model frame as well as the boundary effect. There is no specific engineering background for similar simulation tests. According to the structural characteristics of DCCS, the section shape of the chamber in the geological models is designed as a straight wall semi-circular arch. The section size is 6 × 9 m, and the thickness of the weak stratum is 5 m. The frame size of the plane strain model used in this test is 0.6 × 0.1 × 0.5 m (length × width × height). C_L is 1:50 for the models after a comprehensive evaluation. That is, the section size of the chamber for the coal–gangue separation is 12 × 18 cm in physical models, and the thickness of the weak stratum is 10 cm. Figure 4 shows the laying schemes for the three physical models.

C_γ is calculated based on the actual bulk density of the rock masses and the bulk density of similar materials. The engineering community generally defines rocks with uniaxial compressive strength of less than 25 MPa as weak rocks [28]. The physical and mechanical parameters of rock masses in the geological model are selected concerning relevant references (Table 2) [29,30]. The bulk density of the weak rocks is 2.46 × 10^4 N/m^3. The subsequent proportioning tests of similar materials show that the average bulk density of similar materials for weak rocks is 1.66 × 10^4 N/m^3. Therefore, C_γ is 1:1.48. C_R and C_σ, calculated by Equation (7), are both 1:74. The uniaxial compressive strength of the weak

rocks and other surrounding rocks is calculated by C_R in the physical models and was 0.24 and 1.12 MPa, respectively.

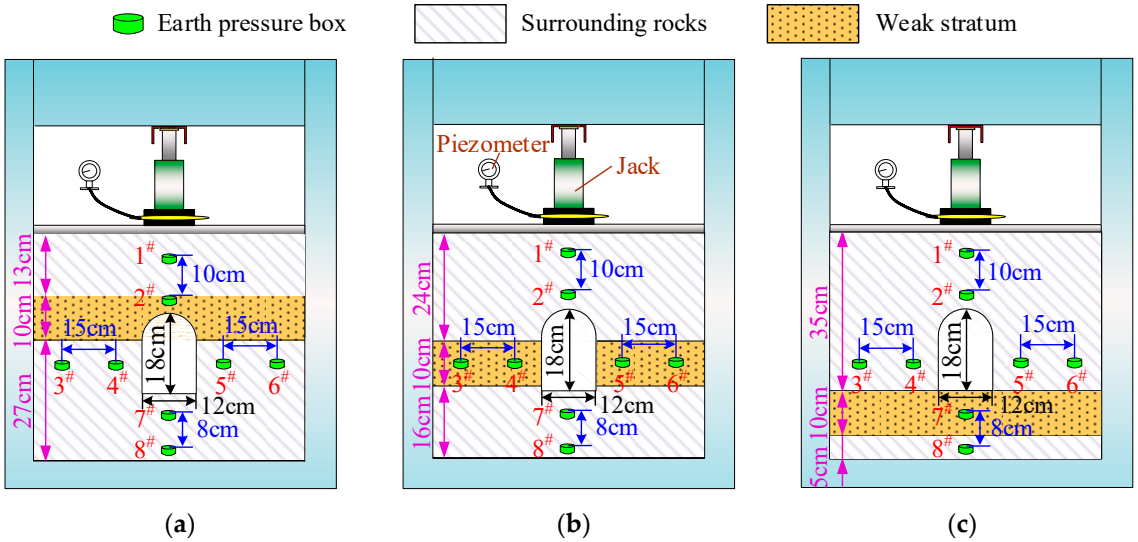

Figure 4. Laying schemes for physical models: (**a**) model 3; (**b**) model 6; (**c**) model 8.

Table 2. Physical and mechanical parameters of the rock stratum in the geological model.

Types of the Rock Strata	Density (kg·m^{-3})	Elastic Modulus (GPa)	Poisson's Ratio	Friction Angle (°)	Cohesion (MPa)	Compressive Strength (MPa)	Tensile Strength (MPa)
Weak rocks	2460	6.4	0.26	30	1.2	18	0.58
Other surrounding rocks	2630	10.1	0.20	38	6.0	83	2.50

3.2. Selection of Similar Materials for the Rock Stratum

The proportioning tests of similar materials should be conducted before laying physical models. The river sand, light calcium carbonate, cement, gypsum, and water are used to configure similar materials in the rock stratum based on previous research and application of similar materials [31,32]. River sands screened by a 2 mm standard sieve are aggregated. The primary function of the light calcium carbonate is to serve as an aggregate and a component that reduces strength. Moreover, cement and gypsum are cementing materials. The cement is made of ordinary Portland cement with a strength mark of C42.5. The proportioning schemes for six groups of similar materials are designed regarding Ref. [16] (Table 3).

Table 3. Proportioning schemes for similar materials.

Number	Proportioning Number	Reference Strength (MPa)	Measured Density (kg·m^{-3})	River Sand (kg)	Light Calcium Carbonate (kg)	Cement (kg)	Gypsum (kg)	Amount of Water
1	773	0.07	1660	0.40	0.12		0.05	1/9
2	737	0.14	1925	0.46	0.06		0.14	1/9
3	337	0.28	2009	0.21	0.14		0.34	1/7
4	937	1.23	1866	0.58		0.02	0.04	1/9.5
5	773	1.55	1955	0.49		0.19	0.06	1/16
6	837	2.06	2024	0.56		0.04	0.10	1/11

Various proportioning materials are made into cube specimens with a side length of 70 mm using molds. Three specimens are made for each proportioning scheme to reduce the discreteness of the test data. All specimens are naturally dried for 1 day after demolding, and then, placed into an oven at 40 °C for drying. Then, the specimens are taken out to

measure the average density of similar materials. Table 3 lists the test results. The uniaxial compressive strength of the specimens is tested by a rigid testing machine at a loading speed of 0.5 mm/min [33]. Figure 5 shows the failure states of specimens with various proportions under uniaxial compression.

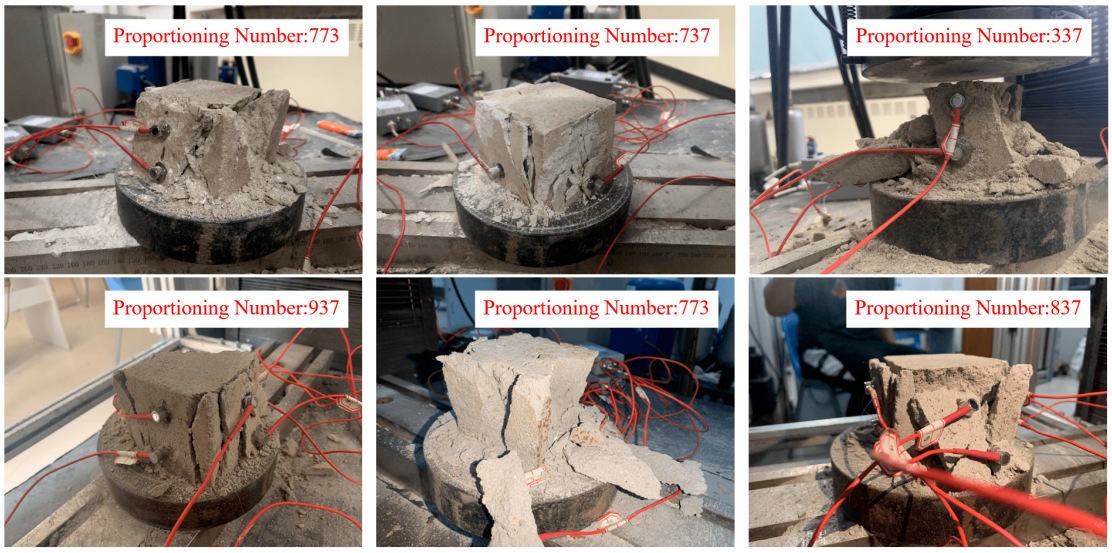

Figure 5. Uniaxial compression tests of specimens with different proportioning schemes.

Figure 6 shows the stress–strain curves of specimens with different proportioning schemes under uniaxial compression. Sample 1, with a proportioning number of 737, experiences fragmentation when the strain exceeds 6×10^{-3}, which prevents the acquisition of subsequent stress–strain data. The test aims to obtain the uniaxial compressive strength of each proportioning material. Sample 1 is at the post-peak stage when fragmentation occurs. Therefore, it does not have any impact on the test results.

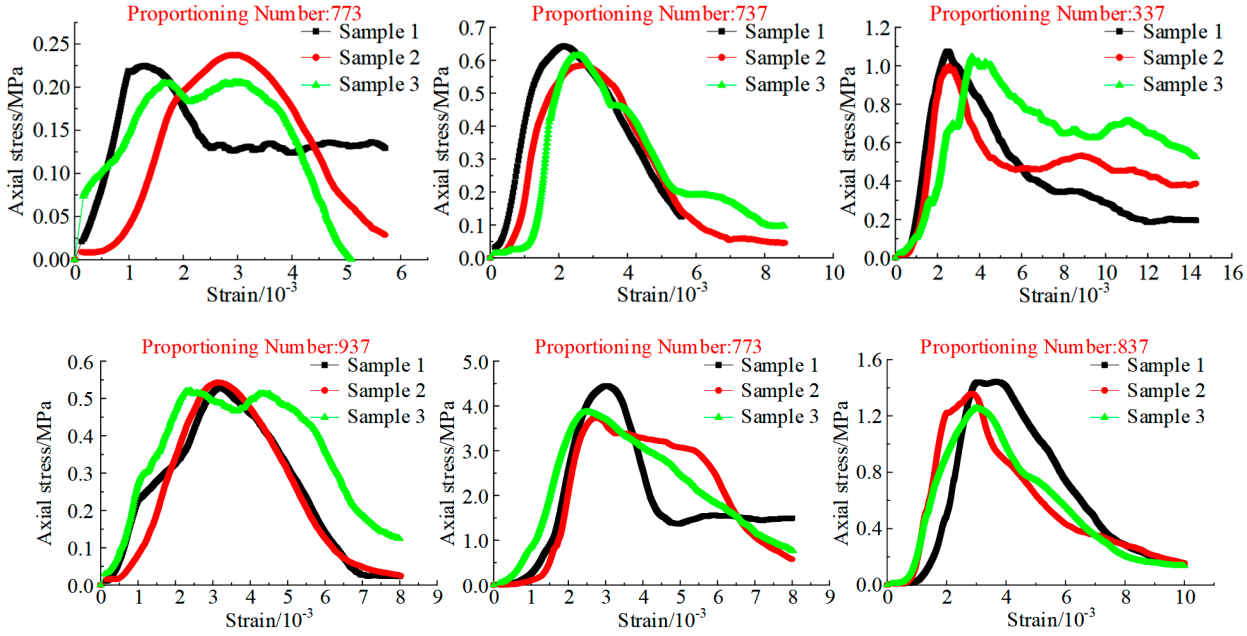

Figure 6. Stress-strain curves of specimens with different proportioning schemes under uniaxial compression.

The average value of the uniaxial compressive strength of three specimens can be calculated. Thereby, the uniaxial compressive strengths of the various proportioning materials

are 0.22, 0.61, 1.03, 0.53, 4.02, and 1.35 MPa, in sequence. The difference between the uniaxial compressive strength and reference strength of similar materials is obvious by comparing Table 3. According to the similarity ratio of strength, a similar material with a proportioning number of 773 is used to simulate weak rocks. Furthermore, a similar material with a proportioning number of 837 is used to simulate the other surrounding rocks.

3.3. Test Scheme and Monitoring Method

Figure 7 shows the physical models laid according to the proportioning schemes for similar materials in the rock stratum. Plexiglass sheets with a thickness of 100 mm are installed at the front and rear sides and reinforced with a steel grating after the model is naturally dried. The frame beams and plexiglass sheets fix the displacement around the model and at the bottom. Hydraulic jacks are used to apply vertical loads to the top of the models to simulate the overlying-stratum stress. The load is determined by converting the pressure gauge reading in the hydraulic pillow.

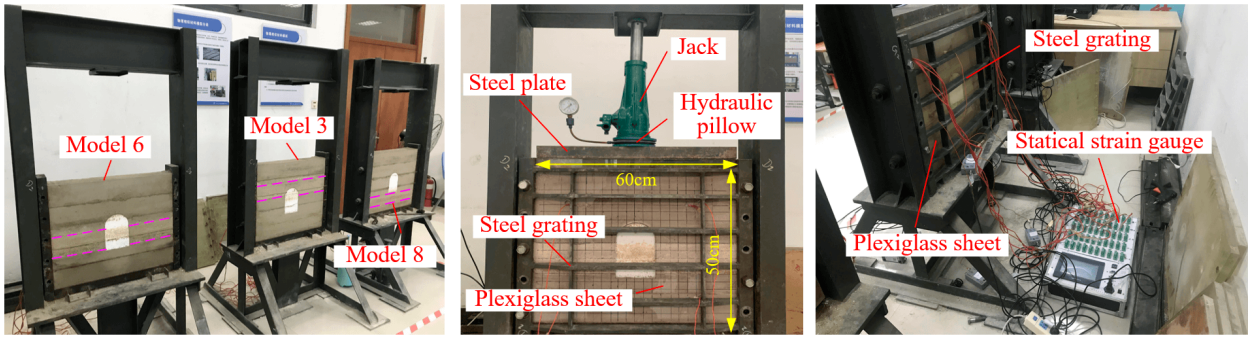

Figure 7. Laying, loading, and monitoring methods for physical models.

Burial depth is designed to be 1000 m at the top of the model due to the research background for deep mining. The load applied to the top of the models is gradually increased from 0 to 0.35 MPa, at an increment of 0.07 MPa, after the chamber is excavated. Eight earth pressure boxes are arranged in each physical model to monitor the evolution law of the stress field in the surrounding rocks. Figure 4 presents the specific location of each earth pressure box. Monitoring data are stored in real-time by a static strain gauge. The deformation and failure of the surrounding rocks are monitored and recorded by drawing grids on the surfaces of the physical models.

3.4. Analysis of Test Results

The evolution law of the stress field in the surrounding rocks of the chamber in the three physical models was analyzed according to the measured data of 1, 3, and 8$^{\#}$ earth pressure boxes in Figure 8. (1) Surrounding rock stress increased with the increased load. Further, the increased stress in the surrounding rocks on the two sides was significantly higher than in the roof and floor. (2) Surrounding rocks near the steel plate inevitably undergo compression failure after initial loadings. As a result, vertical stress monitored by 1$^{\#}$ earth pressure box is always lower than the load value. (3) Based on the monitoring data from 1$^{\#}$ earth pressure box, the descending order of the chamber's roof damage degree was as follows: models 3, 6, and 8. (4) The 3$^{\#}$ earth pressure box was always located in the increased zone of the surrounding rock stress. The damage degree to the surrounding rocks is positively correlated with the stress concentration coefficient. Therefore, the damage degree to the surrounding rocks on the two sides of models 6, 3, and 8 is in descending order. (5) Data obtained from the 8$^{\#}$ earth pressure box indicate that the attenuation of stress in the floors of models 6, 8, and 3 is in descending order.

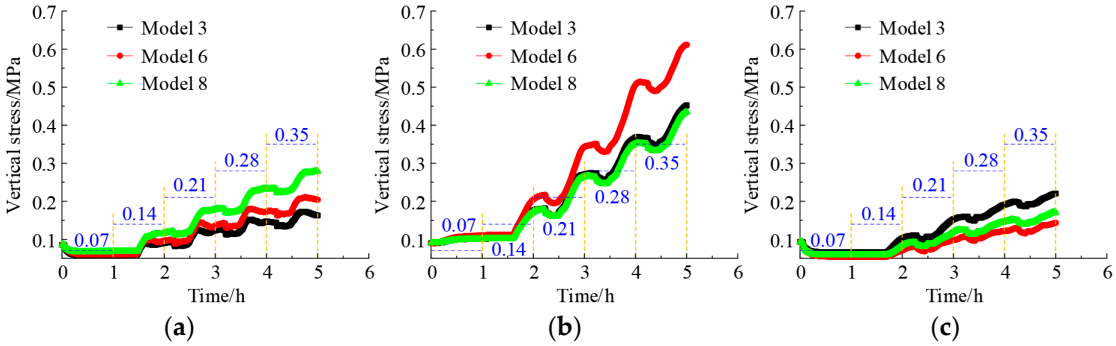

Figure 8. Monitoring results of vertical stress in the surrounding rocks of the chamber at different loading stages: (**a**) the 1# earth pressure box; (**b**) 3# earth pressure box; (**c**) 8# earth pressure box.

The measuring points were separately arranged in the roof, side, and floor of the chamber to monitor the evolution of the displacement field in the surrounding rocks during the loading process. Figure 9 shows the results. (1) The maximum displacement of the surrounding rocks was in the weak stratum. (2) The growth rate of the surrounding rock displacement significantly increased when the load increased from 0.14 MPa. (3) The descending order is characterized in the following aspects, i.e., the roof displacements in models 3, 6, and 8 were under the same loading, the surrounding rock displacements in the side of models 6, 8, and 3, and the floor displacements in models 8, 3, and 6.

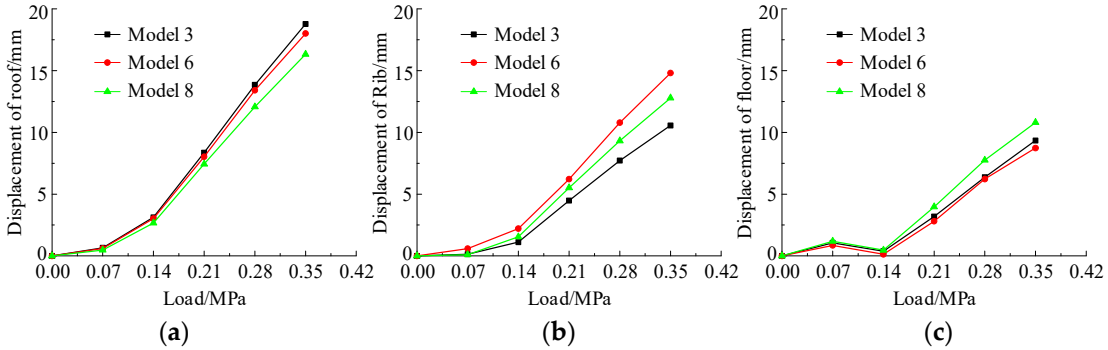

Figure 9. Monitoring results on surrounding rock displacements at different loading stages: (**a**) roof displacement; (**b**) surrounding rock displacement in the sides; (**c**) floor displacement.

Figure 10 shows the deformation and failure in the surrounding rocks of the chamber at each loading stage. (1) The weak stratum first fails within each physical model during the loading. (2) When the weak stratum is located in the roof, axial tensile cracks first occur in the middle of the roof with increased loads. Then, the roof experiences penetrating failure and bending deflection. As a result, the rock masses at the shoulder arch undergo tensile-fracture failure. The broken blocks engage with each other by friction and gradually slide off. Surrounding rocks on two sides finally experience wedge failure due to the weakened constraint effect. (3) When a weak stratum is located on two sides, the weak rocks in the free surface first undergo buckling failure under the extrusion of the roof and floor. The buckling failure by the weak rocks gradually increases as the load increases, and the damage range inside the weak rocks gradually expanded. Ultimately, the weak rocks exhibit a concave failure pattern. (4) The floor first generates tensile cracks during loading, when a weak stratum is located in the floor. Next, the floor eventually swells and damages through the development of tensile cracks. As a result, constraints to the surrounding rocks on the side near the floor become weakened, and the surrounding rocks on the two sides undergo wedge failure. (5) The deformation and failure of the surrounding rocks in the chamber in models 3, 6, and 8 are in descending order under the same loading.

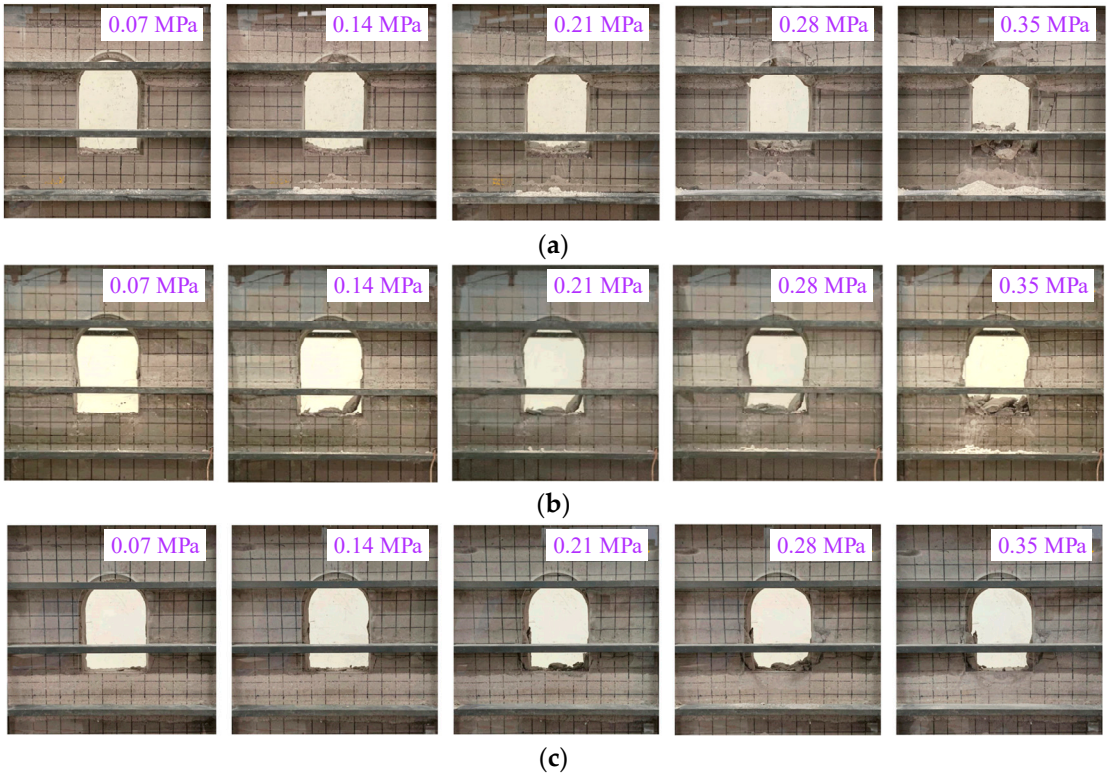

Figure 10. Failure modes in the surrounding rocks of the chamber at different loading stages: (**a**) model 3; (**b**) model 6; (**c**) model 8.

4. Numerical Simulation

4.1. Numerical Simulation Schemes

The similar simulation tests mentioned earlier cannot consider the lateral pressure coefficient as a key factor. Therefore, 15 groups in the plane-strain numerical models for DCCS are established using FLAC^{3D} 6.0 software (Figure 3). Figure 11 shows the dimensions and boundary conditions in the numerical model. Normal-displacement constraints are applied to the periphery and bottom of the model. The thickness of the weak stratum is 5 m in models 3 to 8, and the thickness of the weak stratum is 2 m in models 9 to 15. The Mohr–Coulomb constitutive model is applied to all numerical models.

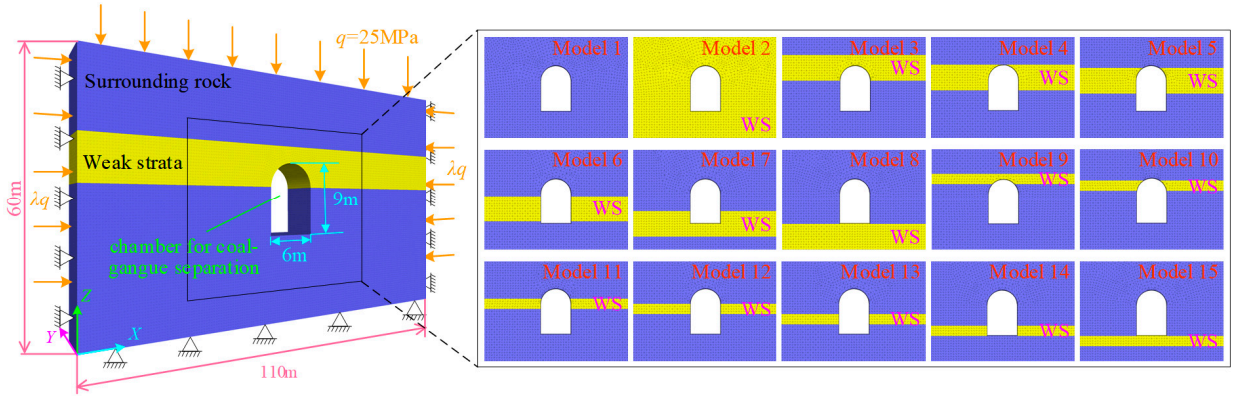

Figure 11. Plane-strain numerical models of DCCS. Note: WS represents a weak stratum.

Table 2 lists the physical and mechanical parameters of the rock masses. Numerical calculations follow the software's default convergence standards. Vertical stress applied to the top of the models is 25 MPa, and horizontal stress is specifically determined by the

lateral pressure coefficient λ, whereby λ is 0.6, 1.0, 1.4, and 1.8. There is a total of 60 sets of numerical simulation schemes.

The reliability of the numerical simulations should be verified. To this end, numerical calculations are performed based on a similar simulation test. The distribution characteristics of the vertical stress and plastic zone in the surrounding rocks of DCCS are finally obtained (Figure 12). The distribution law of the vertical stress in three numerical models is consistent with similar simulation results by comparing Figures 8 and 12a. Meanwhile, Figures 10 and 12b show that the damage and failure characteristics of the weak stratum and its adjacent surrounding rocks in the numerical models are approximately the same as those in the physical models. Therefore, the numerical simulation results can be considered reliable.

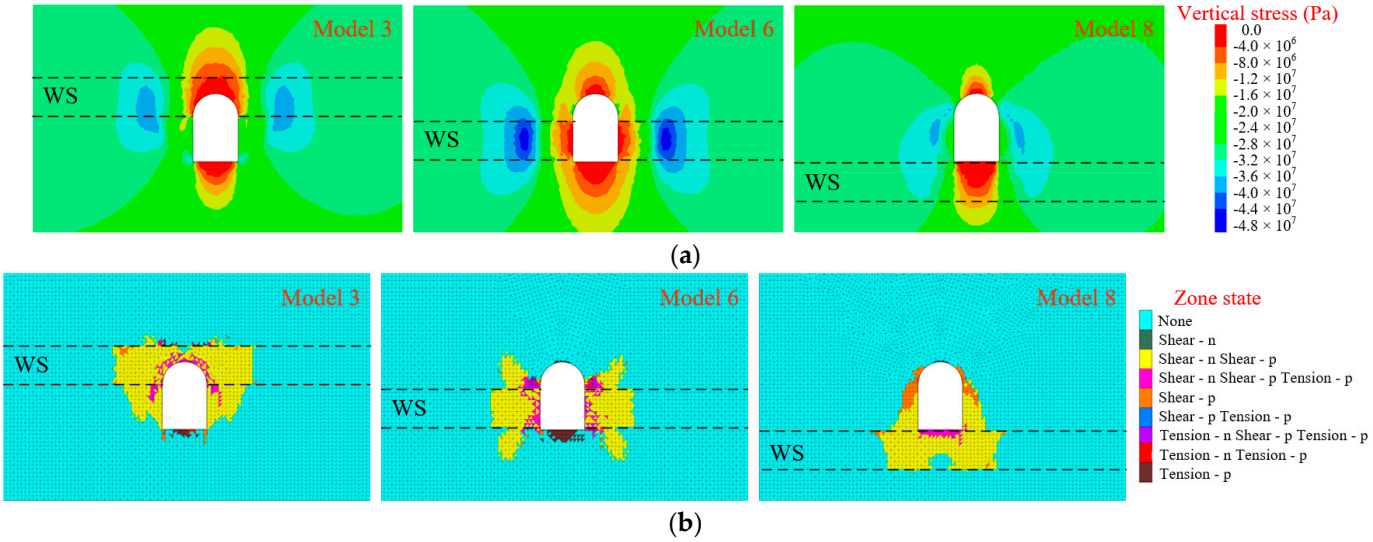

Figure 12. Distribution characteristics of vertical stress and plastic zone in three numerical models. (**a**) Distribution of vertical stress; (**b**) distribution of plastic zone. Note: WS represents a weak stratum.

4.2. Analysis of Numerical Simulations

Figure 13 shows the plastic failure range and displacement distribution characteristics in the surrounding rocks of DCCS in each scheme when λ is 1.0. PFA is the plastic failure area in the surrounding rocks within the section calculated by the self-programmed FISH program. (1) The plastic failure range and maximum displacement of the surrounding rocks are positively correlated with the thickness of the weak stratum. The maximum displacement of the surrounding rocks occurs in the weak rocks on the free surface. (2) The constraint effect on the adjacent surrounding rocks is weakened after the failure of the weak stratum. It results in a wedge-shaped failure in the adjacent surrounding rocks, which is consistent with the results of similar simulation tests. (3) The plastic failure range of the surrounding rocks is the largest when the roof of DCCS is arranged along the weak stratum. The maximum displacement of the surrounding rocks reaches the peak when the floor of DCCS is arranged along the weak stratum. (4) There is no direct correspondence between the plastic failure range of the surrounding rocks and the maximum displacement. For example, the plastic failure range of the surrounding rocks in model 4 is larger than in model 5. However, the maximum displacement of the surrounding rocks in model 4 is smaller than in model 5. (5) The plastic failure range of the surrounding rocks in model 8 is at its minimum when the thickness of the weak stratum is 5 m. Moreover, the maximum displacement of the surrounding rocks in model 7 is the minimum value. (6) The plastic failure range and maximum displacement of the surrounding rocks in model 14 are both the minimum values when the thickness of the weak stratum is 2 m.

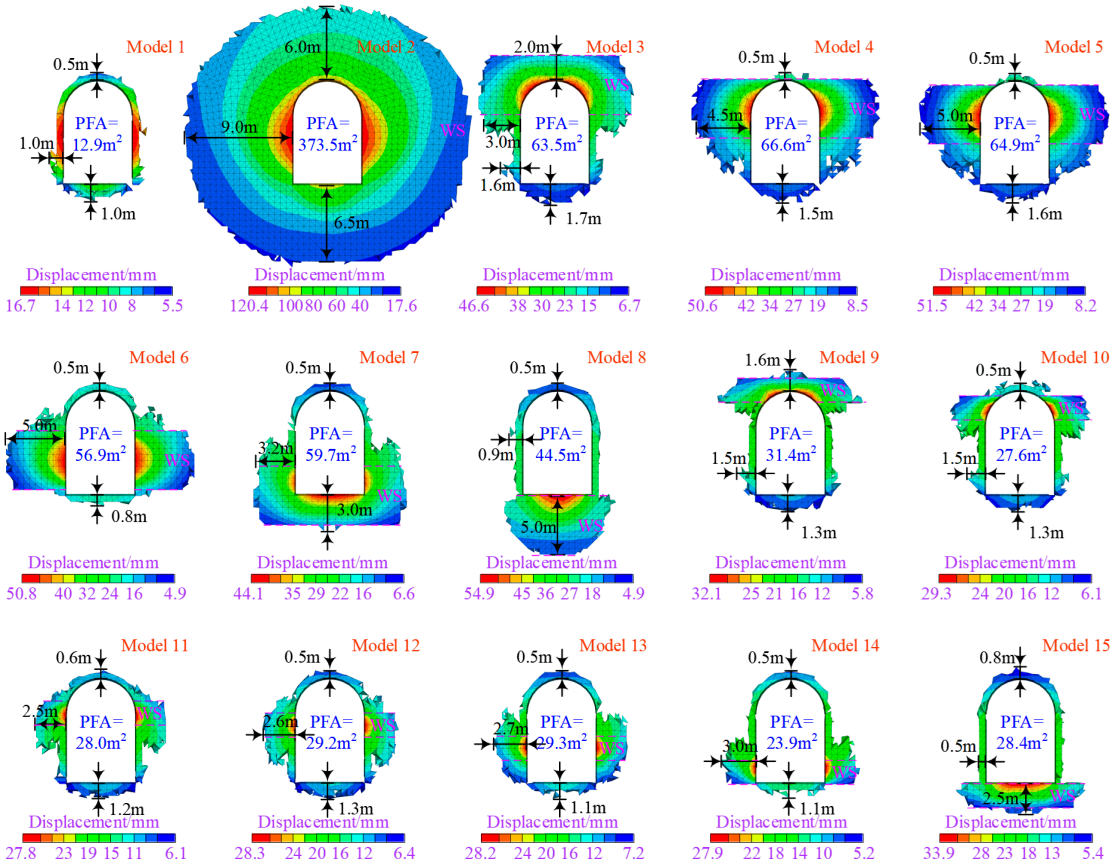

Figure 13. Plastic failure range and displacement distribution characteristics for the surrounding rocks of DCCS under different weak stratum horizons.

Figure 14 shows the variation curves for the PFA in the surrounding rocks under different lateral pressure coefficients. (1) The tensile failure area (TFA) and the PFA are always positively correlated with the thickness of the weak stratum. (2) When the thickness of the weak stratum is 5 m, the TFA and PFA in the surrounding rocks in model 8 are at their minimum when $0.6 \leq \lambda \leq 1.4$. The floor of DCCS arranged along the weak stratum is beneficial in reducing the plastic failure range of the surrounding rocks. (3) When the thickness of the weak stratum is 5 m, the TFA and PFA in the surrounding rocks in model 6 are at their minimum if λ is 1.8. The two sides of DCCS are arranged along the weak stratum and are most conducive to reducing the plastic failure range in the surrounding rocks. (4) When the thickness of the weak stratum is 2 m, the TFA and PFA in the surrounding rocks in model 14 are at their minimum when $0.6 \leq \lambda \leq 1.4$. Arranging the side near the floor of DCCS along the weak stratum is most conducive to reducing the plastic failure range in the surrounding rocks when the thickness of the weak stratum is small. (5) If the thickness of the weak stratum is 2 m and λ is 1.8, the plastic failure range of the surrounding rocks is the minimum when the weak stratum is located in the middle of the side.

Figure 15 shows the variation in the curves of the surrounding rock convergence. (1) The location of the weak stratum is the maximum deformation area in the surrounding rocks and it is consistent with the results of similar simulation tests. (2) The convergence of the roof and floor is the maximum when the weak stratum is located on the floor. (3) The convergence of the two sides is proportional to λ. (4) When the thickness of the weak stratum is 5 m and λ is 0.6, the horizon of the weak stratum has little effect on the convergence of the roof and floor. (5) The displacement of the weak stratum in model 7 is the lowest when $0.6 \leq \lambda \leq 1$ and the thickness of the weak stratum is 5 m. Furthermore, the displacement of the weak stratum in model 6 is the lowest when $\lambda \geq 1.4$. (6) The displacement of the weak stratum in model 14 is the smallest when $0.6 \leq \lambda \leq 1$ and the

thickness of the weak stratum is 2 m. Furthermore, the displacement of the weak stratum in model 12 is the lowest when $\lambda \geq 1.4$.

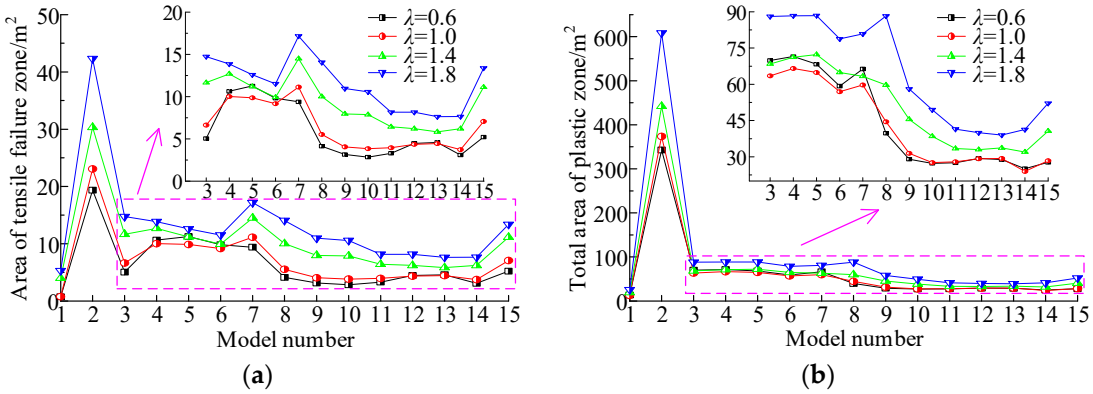

Figure 14. Variation curves in the plastic failure range of the surrounding rocks under different weak stratum horizons: (**a**) tensile failure area; (**b**) plastic failure area.

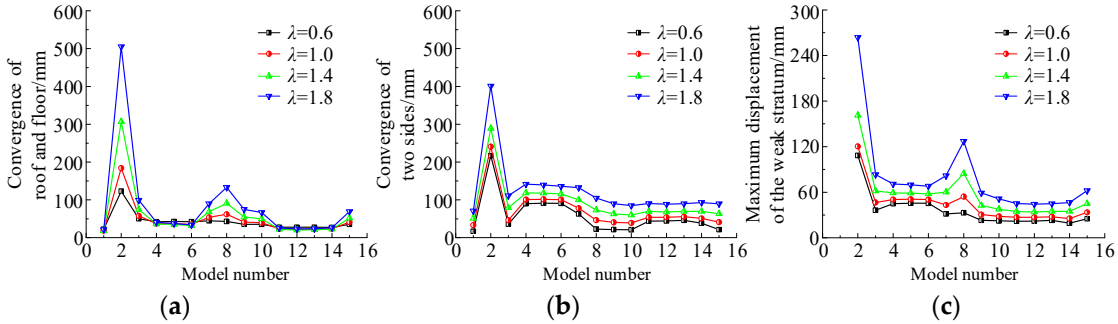

Figure 15. Variation curves in the surrounding rock convergence under different horizons of the weak stratum: (**a**) convergence of roof and floor; (**b**) convergence of two sides; (**c**) maximum displacement of the weak stratum.

When the lateral pressure coefficient and the thickness of the weak stratum are constant, the model with the minimum plastic failure range in the surrounding rocks is not completely consistent with the model with the lowest convergence in the surrounding rocks. A comprehensive evaluation coefficient of the surrounding rock stability is proposed to quantitatively evaluate the optimal layout method of DCCS based on the weak stratum horizon. When λ is 1, the following parameters are taken as reference quantities separately, i.e., the convergence of the roof and floor, the convergence of the two sides, the maximum displacement of the weak stratum, and the PFA in the surrounding rocks of DCCS in model 3. The ratio of each quantity in other models to the corresponding reference quantity is defined as the evaluation factor of the surrounding rock stability. The comprehensive evaluation coefficient of the surrounding rock stability is obtained by multiplying the evaluation factors. Figure 16 shows the calculation results for the comprehensive evaluation coefficients in all models.

The following results can be obtained based on Figure 16. (1) If the thickness of the weak stratum is large, the floor of DCCS arranged along the weak stratum is the most conducive to the surrounding rock control when $0.6 \leq \lambda \leq 1$. The stability of the surrounding rock is optimal with the side of DCCS arranged along the weak stratum and $\lambda > 1$. (2) If the thickness of the weak stratum is small, the side near the floor of DCCS arranged along the weak stratum is the most conducive to the surrounding rock stability with $0.6 \leq \lambda \leq 1$. The stability of the surrounding rock is optimal when the side near the roof of DCCS is arranged along the weak stratum and $\lambda > 1$.

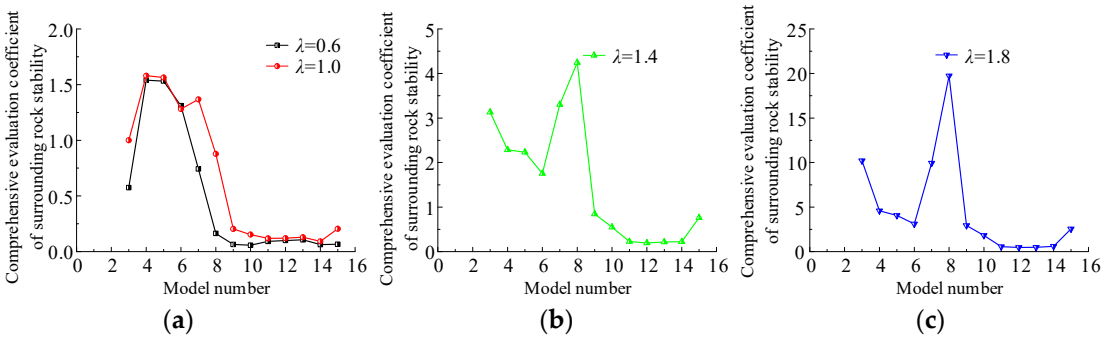

Figure 16. Variation curves for the comprehensive evaluation coefficients of the surrounding rock stability: (**a**) λ is 0.6 or 1.0; (**b**) λ is 1.4; (**c**) λ is 1.8.

The following conclusions can be briefly summarized according to the simulation results. The thickness of the weak stratum is a key factor affecting the surrounding rock stability of DCCS. The DCCS should be arranged as far as possible in areas where there is no weak stratum, or the thickness of the weak stratum is small. The influence of the weak stratum and its horizon on the surrounding rock stability varies significantly under different lateral pressure coefficients. Therefore, the in situ stress test should be conducted first to determine the value of the lateral pressure coefficient before DCCS is arranged. It should be avoided to arrange the roof and floor of DCCS along the weak stratum as much as possible when $\lambda < 0.6$ or $\lambda > 1$. The bottom of DCCS is arranged along a weak stratum when $0.6 \leq \lambda \leq 1$, which is most conducive to the control of the surrounding rock. The weak stratum and its adjacent surrounding rocks are key areas that need to be reinforced after the excavation of DCCS. The evaluation method for the surrounding rock stability proposed in this work belongs to comprehensive judgment criteria. The layout methods of DCCS based on the horizon of the weak stratum can also be flexibly selected according to the actual situation of the mine or the key points of the surrounding rock control (the plastic failure range and maximum convergence).

5. Discussion

The work does not consider the cases of $\lambda < 0.6$ and $\lambda > 1.8$ in numerical simulations. We have studied the plastic failure characteristics for the surrounding rocks of DCCS in both cases at the early stage. The research results show that the degree of damage to the roof and floor is significantly greater than for the two sides when $\lambda < 0.6$ and $\lambda > 1.8$. In other words, the current key areas in controlling the surrounding rock are the roof and the floor. Therefore, the optimal layout methods of DCCS based on the horizon of the weak stratum when $\lambda < 0.6$ or $\lambda > 1.8$ are consistent with that when $\lambda > 1$.

At present, there are few related studies on the influence of the horizon of the weak stratum on the stability of the surrounding rocks in roadways and chambers. Ref. [34] analyzed the instability characteristics and failure forms in roofs under different horizons of the weak stratum. According to the different horizons in the weak stratum, hierarchical reinforcement control measures for the roof are proposed. Ref. [35] points out that the surrounding rock deformation and stress concentration are relatively small when the weak stratum is located on the floor or the side near the floor. Moreover, the stability of the surrounding rock is optimal when the weak stratum is located on the side near the floor.

The above research is of great significance for guiding engineering practices. However, the research object does not involve a roadway or chamber with structural features of a small width-to-height ratio. Meanwhile, the optimal layout methods for the roadway or chamber, which are based on the weak stratum horizon in different ground stresses, have not been specified. Therefore, the optimal layout methods of DCCS based on the horizon of the weak stratum proposed in the work can provide a reference for engineering practices. The research results have relatively great potential for application in deep resource mining.

Note that the spatial layout of DCCS is constrained by other geological factors, such as faults, structural planes, and groundwater. The weak stratum is taken as the main research object, meaning that the influence of other geological factors on the stability of the surrounding rock of DCCS was not considered. In the future, we will use numerical simulation as the main research method to explore the optimal layout methods of DCCS based on the above three geological factors.

6. Conclusions

Determining the optimal layout methods of DCCS based on the weak stratum horizon is of great significance for reducing the difficulties in controlling the surrounding rock and ensuring safe and efficient mining conditions. The work summarized the main structural characteristics of underground chambers in coal–gangue separations. The deformation and failure characteristics of rocks surrounding DCCS under different weak stratum horizons were revealed by similar simulation tests. A comprehensive evaluation method for the surrounding rock stability was proposed. Finally, numerical simulations were used to determine the optimal layout methods of DCCS based on the horizon of the weak stratum. The main conclusions are as follows.

(1) The structural characteristics of the DCCS included a large cross-section, a small ratio of width to height, and a significantly larger axial length than the cross-sectional size.
(2) The results of similar simulation tests indicate that the weak rocks near the free surface initially underwent deformation and failure after DCCS was excavated. The adjacent surrounding rocks underwent wedge failure due to the weakened restraint effect after the weak rocks failed. Therefore, timely implementation of measures, such as increasing the length of the rock bolts, reducing the spacing between the rock bolts, and grouting were imperative to enhancing the support for weak rocks and their adjacent surrounding rock formations. Surrounding rocks were maintained in a stress equilibrium state as a whole to produce uniform and coordinated deformations.
(3) The lateral pressure coefficient λ and the thickness and horizon of the weak stratum affected the surrounding rock stabilities of DCCS. The in situ stress test should be conducted first to determine the lateral pressure coefficient before planning DCCS. Meanwhile, the thickness and horizon of the weak stratum should be clearly defined based on the bore histogram. Numerical simulation results indicated that the plastic failure range and maximum displacement of the surrounding rocks were positively correlated with the thickness of the weak stratum. The plastic failure range of the surrounding rocks was the largest when the roof of DCCS was arranged along the weak stratum. Moreover, the maximum displacement of the surrounding rocks reached its peak when the floor of DCCS was arranged along the weak stratum. The convergence of the two sides was proportional to λ. Therefore, the axial direction of DCCS should be arranged as parallel or inclined as possible to the direction of the maximum horizontal principal stress.
(4) If the thickness of the weak stratum was small, the side near the roof of DCCS should be arranged along the weak stratum when $\lambda < 0.6$ or $\lambda > 1$. Additionally, the side near the floor of DCCS was arranged along the weak stratum when $0.6 \leq \lambda \leq 1$, and the stability of the surrounding rocks was optimal. If the thickness of the weak stratum was large, the side of DCCS should be arranged along the weak stratum when $\lambda < 0.6$ or $\lambda > 1$. The floor of DCCS was arranged along the weak stratum when $0.6 \leq \lambda \leq 1$, which was most conducive to controlling the surrounding rocks.
(5) According to the actual situation of the mine or the key points of the surrounding rock control (the plastic failure range and maximum convergence), the layout methods of DCCS based on the weak stratum horizon could be flexibly selected regarding the simulation results.

Author Contributions: All authors contributed extensively to the work. C.Z. and Y.Y. proposed key ideas. H.S. provided practice guidance in the research process. C.Z. and Z.C. contributed to field measurements. C.Z., Z.C. and W.W. mainly completed similar simulation tests and numerical simulations. Z.C. and W.W. analyzed the data. C.Z. wrote the paper. C.Z. and H.S. modified the manuscript. All authors have read and agreed to the published version of the manuscript.

Funding: This work was funded by the Research Fund of Key Laboratory of Deep Coal Resource Mining (CUMT), Ministry of Education (Grant No. KLDCRM202205), and the National Natural Science Foundation of China (Grant No. 51974294).

Institutional Review Board Statement: Not applicable.

Informed Consent Statement: Not applicable.

Data Availability Statement: The data that support the findings of this study are available on request from the corresponding author. The data are not publicly available due to privacy orethical restrictions.

Conflicts of Interest: The authors declare no conflict of interest.

References

1. Xie, H.P.; Ju, Y.; Ren, S.H.; Gao, F.; Liu, J.Z.; Zhu, Y. Theoretical and technological exploration of deep in situ fluidized coal mining. *Front. Energy* **2019**, *13*, 603–611. [CrossRef]
2. Zhao, Z.H.; Tan, Y.L.; Chen, S.J.; Ma, Q.; Gao, X.J. Theoretical analyses of stress field in surrounding rocks of weakly consolidated tunnel in a high-humidity deep environment. *Int. J. Rock Mech. Min. Sci.* **2019**, *122*, 104064. [CrossRef]
3. Zhang, J.X.; Zhang, Q.; Spearing, A.J.S.; Miao, X.A.; Guo, S.; Sun, Q. Green coal mining technique integrating mining-dressing-gas draining-backfilling-mining. *Int. J. Min. Sci. Technol.* **2017**, *27*, 17–27. [CrossRef]
4. Zhang, Q.; Kang, Y.; Zhang, J.X.; Yin, W.; Liu, X.W.; Wu, Z.Y.; Song, W.J.; Xu, X.L. Monitoring and measurement analysis of key indexes for the implementation of mining, dressing, backfilling, and controlling technology in coal resources—A case study of Tangshan Mine. *Energy Sci. Eng.* **2022**, *10*, 680–693.
5. Zhang, Q.; Zhang, J.X.; Tai, Y.; Fang, K.; Yin, W. Horizontal roof gap of backfill hydraulic support. *J. Cent. South Univ.* **2015**, *22*, 3544–3555. [CrossRef]
6. Zhang, J.X.; Miao, X.X.; Zhang, Q.; Zhang, J.G.; Yan, H. Integrated coal and gas simultaneous mining technology: Mining-dressing-gas draining-backfilling. *J. China Coal Soc.* **2016**, *41*, 1683–1693. (In Chinese)
7. Yuan, Y.; Yuan, C.F.; Zhu, C.; Wang, P. Mechanical model and application of the deformation cylinder of the surrounding rock in the deep large section chamber. *J. Min. Saf. Eng.* **2020**, *37*, 338–348. (In Chinese)
8. Zhu, C.; Yuan, Y.; Wang, W.M.; Chen, Z.S.; Wang, S.Z.; Zhong, H.W. Research on the "three shells" cooperative support technology of large-section chambers in deep mines. *Int. J. Min. Sci. Technol.* **2021**, *31*, 665–680. [CrossRef]
9. Tan, Y.L.; Fan, D.Y.; Liu, X.S.; Song, S.L.; Li, X.F.; Wang, H.L. Numerical investigation of failure evolution for the surrounding rock of a super-large section chamber group in a deep coal mine. *Energy Sci. Eng.* **2019**, *7*, 3124–3146. [CrossRef]
10. Fan, D.Y.; Liu, X.S.; Tan, Y.L.; Li, X.B.; Lkhamsuren, P. Instability energy mechanism of super-large section crossing chambers in deep coal mines. *Int. J. Min. Sci. Technol.* **2022**, *32*, 1075–1086. [CrossRef]
11. Zhai, X.X.; Huang, G.S.; Chen, C.Y.; Li, R.B. Combined supporting technology with bolt-grouting and floor pressure-relief for deep chamber: An underground coal mine case study. *Energies* **2018**, *11*, 67. [CrossRef]
12. Liu, X.S.; Fan, D.Y.; Tan, Y.L.; Song, S.L.; Li, X.F.; Ning, J.G.; Gu, Q.H.; Ma, Q. Failure evolution and instability mechanism of surrounding rock for close-distance parallel chambers with super-large section in deep coal mines. *Int. J. Geomech.* **2021**, *21*, 04021049. [CrossRef]
13. Sun, X.M.; Wang, D.; Miao, C.Y.; Li, Y.; Xu, H.C. Research on dynamic pressure instability mechanism and control countermeasure of deep pump room and chamber group in Nantun Coal Mine. *J. China Coal Soc.* **2015**, *40*, 2303–2312. (In Chinese)
14. Jia, S.P.; Yang, J.W.; Gao, M.; Jia, L.F.; Wen, C.X.; Wu, G.J. Experimental and numerical analysis of deformation and failure behaviour for deep roadways in soft rocks. *Bull. Eng. Geol. Environ.* **2022**, *81*, 466. [CrossRef]
15. Liu, H.Y.; Liu, C.W.; Zhai, M.H.; Zhang, P.; Wang, L.J.; Wang, F.; Liu, J.A. Collaborative control technology of crosscut floor heave in soft rocks under deep high horizontal stress. *Math. Probl. Eng.* **2022**, *2022*, 1–13. [CrossRef]
16. Liu, X.S.; Song, S.L.; Tan, Y.L.; Fan, D.Y.; Ning, J.G.; Li, X.B.; Yin, Y.C. Similar simulation study on the deformation and failure of surrounding rock of a large section chamber group under dynamic loading. *Int. J. Min. Sci. Technol.* **2021**, *31*, 495–505. [CrossRef]
17. Kang, H.P.; Wang, J.H.; Lin, J. Case studies of rock bolting in coal mine roadways. *Chin. J. Rock Mech. Eng.* **2010**, *29*, 649–664. (In Chinese)
18. Tan, Y.L.; Fan, D.Y.; Liu, X.S.; Li, X.F.; Ma, Q.; Wang, H.L.; Fan, W.C. Discrimination method and engineering characteristics of super large section chamber in coal mine. *J. Min. Saf. Eng.* **2020**, *37*, 23–31. (In Chinese)
19. Yuan, L.; Xue, J.H.; Liu, Q.S.; Liu, B. Surrounding rock stability control theory and support technique in deep rock roadway for coal mine. *J. China Coal Soc.* **2011**, *36*, 535–543. (In Chinese)
20. Li, Z.X.; Zhang, Y.D.; Ma, Q.; Zheng, Y.; Song, G.Y.; Yan, W.Z.; Zhang, Y.; Hu, L. The floor heave mechanism and control technology of gob-side entry retaining of soft rock floor. *Sustainability* **2023**, *15*, 6074. [CrossRef]

21. Xie, S.R.; Jiang, Z.S.; Chen, D.D.; Wang, E. Study on zonal cooperative control technology of surrounding rock of super large section soft rock chamber group connected by deep vertical shaft. *Adv. Civ. Eng.* **2022**, *2022*, 4220998. [CrossRef]
22. Zhang, W. Study on stress disturbed mechanism and supporting method of weakly cemented roadway near chambers. *Complexity* **2023**, *2023*, 7775116. [CrossRef]
23. Yuan, Y.; Liu, Z.H.; Zhu, C.; Yuan, C.F.; Wang, S.Z. The effect of burnt rock on inclined shaft in shallow coal seam and its control technology. *Energy Sci. Eng.* **2019**, *7*, 1882–1895. [CrossRef]
24. Ma, Q.; Zhang, Y.D.; Li, Z.X.; Zheng, Y.; Song, G.Y.; Hu, L. The optimized roadway layouts and surrounding rock control technology of the fully mechanized mining surface with large mining heights in high-gas mines. *Processes* **2022**, *10*, 2657. [CrossRef]
25. Li, G.; Sun, Q.H.; Ma, F.S.; Guo, J.; Zhao, H.J.; Wu, Y.F. Damage evolution mechanism and deformation failure properties of a roadway in deep inclined rock strata. *Eng. Fail. Anal.* **2023**, *143*, 106820. [CrossRef]
26. Han, P.H.; Zhang, C.; Ren, Z.P.; He, X.; Jia, S. The influence of advance speed on overburden movement characteristics in longwall coal mining: Insight from theoretical analysis and physical simulation. *J. Geophys. Eng.* **2021**, *18*, 163–176. [CrossRef]
27. Wang, W.M.; Yuan, Y.; Chen, Z.S.; Zhu, C. Physical modeling of floor failure above confined water: A case study in China. *Environ. Earth Sci.* **2022**, *81*, 325. [CrossRef]
28. Kang, H.P.; Yi, K. Simulation study on dilatant and rheologic properties of soft rocks surrounding deep roadway and its application. *J. China Coal Soc.* **2023**, *48*, 15–33. (In Chinese)
29. Ma, X.M.; Xue, Y.G.; Qiu, D.H.; Xia, T.; Qu, C.Q.; Kong, F.M. Classification for tunnel surrounding rock based on multiple geological methods and extension model. *Bull. Eng. Geol. Environ.* **2023**, *82*, 109. [CrossRef]
30. He, X.; He, S.X.; Cai, Y.B.; Xu, R.Y.; Yang, K. Investigation on rational width of coal pillar and roadway support in isolated panel of extra-thick coal seam. *Front. Earth Sci.* **2023**, *11*, 1125678. [CrossRef]
31. Zhu, Z.G.; Fang, Z.C.; Xu, F.; Han, Z.M.; Guo, X.L.; Ma, C.Y. Model test study on the rock mass deformation law of a soft rock tunnel under different ground stresses. *Front. Earth Sci.* **2022**, *10*, 962445. [CrossRef]
32. Ning, J.G.; Wang, J.; Bu, T.T.; Hu, S.C.; Liu, X.S. An innovative support structure for gob-side entry retention in steep coal seam mining. *Minerals* **2017**, *7*, 75. [CrossRef]
33. Wang, C.; Zhu, C.; Yuan, Y.; Chen, Z.S.; Wang, W.M. Study on the working resistance of a support under shallowly buried gobs according to the roof structure during periodic weighting. *Sustainability* **2021**, *13*, 10652. [CrossRef]
34. Zhang, N.; Li, G.C.; Kan, J.G. Influence of soft interlayer location in coal roof on stability of roadway bolting structure. *Rock Soil Mech.* **2011**, *32*, 2753–2758. (In Chinese)
35. Zhang, Y.G.; Tu, M. The effect of weak interlayer horizon on roadway surrounding rock stability. *Saf. Coal Mines* **2014**, *45*, 216–218. (In Chinese)